MICROBIOLOGY

# Terpenoid balance in *Aspergillus nidulans* unveiled by heterologous squalene synthase expression

**Sung Chul Park[1], Breanne N. Steffan[1], Fang Yun Lim[1,2], Raveena Gupta[3], Fatma Ayaloglu Butun[3], Hongyu Chen[4], Rosa Ye[4], Timothy Decker[4], Chengcang C. Wu[4], Neil L. Kelleher[3], Jin Woo Bok[1]*, Nancy P. Keller[1,5]***



**Filamentous fungi produce numerous uncharacterized natural products (NPs) that are often challenging to characterize because of cryptic expression in laboratory conditions. Previously, we have successfully isolated novel NPs by expressing fungal artificial chromosomes (FACs) from a variety of fungal species into *Aspergillus nidulans*. Here, we demonstrate a twist to FAC utility wherein heterologous expression of a *Pseudogymnoascus destructans* FAC in *A. nidulans* altered endogenous terpene biosynthetic pathways. In contrast to wild type, the FAC transformant produced increased levels of squalene and aspernidine type compounds, including three new nidulenes (1– 2, and 5), and lost nearly all ability to synthesize the major *A. nidulans* characteristic terpene, austinol. Deletion of a squalene synthase gene in the FAC restored wild-type chemical profiles. The altered squalene to farnesyl pyrophosphate ratio leading to synthesis of nidulenes and aspernidines at the expense of farnesyl pyrophosphate–derived austinols provides unexpected insight into routes of terpene synthesis in fungi.**

## INTRODUCTION

Fungi produce a wide variety of natural products (NPs; also called secondary metabolites), some of which have important medicinal properties as drug candidates (*1*–*3*). Among these metabolites, meroterpenoids have emerged as a class of secondary metabolites that have complex structures and diverse bioactivities (*4*, *5*). Meroterpenoids are formed through the mixing of terpene biosynthetic pathways with other biosynthetic origins, such as polyketide or nonribosomal peptide pathways, resulting in a high degree of structural diversity (*4*, *6*). These compounds have attracted substantial attention in drug discovery and development due to promising pharmacological activities, including antifungal, antibacterial, antiviral, anti-inflammatory, and anticancer properties (*7*). More than 1500 novel fungi–derived meroterpenoids have been isolated and published since 2009 (*8*). Hence, understanding the biosynthesis, structure, and biological activities of fungal meroterpenoids is of great interest to the field of drug discovery.

One limitation of current drug discovery in fungi is the difficulty in expressing silent fungal biosynthetic gene clusters (BGCs) under laboratory conditions to produce NPs for drug candidate screening (*9*). Fungal artificial chromosomes (FACs) represent a genetic tool to produce unknown fungal NPs by transforming randomly sheared genomic DNA containing fungal BGCs in heterologous hosts, such as *Aspergillus nidulans* (*10*). FACs offer the advantages of the easy association of mass spectrometry (MS) detectable metabolites with their transformed BGCs (*10*). Many FAC-derived NPs are cryptic metabolites not typically produced by the endogenous species, resulting in an increased potential to find novel fungal metabolites and related BGCs (*11*). For example, benzomalvins A/D (*11*), valactamide A (*11*), and terreazepine (*12*) and their BGCs were newly identified by applying FACs transformation into *A. nidulans*.

*A. nidulans* is a renowned heterologous expression host due to the ease of genetic manipulation first established in the late 1940s (*13*) and easily adapted to new genetic tools in the subsequent decades (*14*). Further, studies in this fungus in the past 30 years have linked over 30 BGCs to specific NPs (*15*), which simplifies the identification of heterologous NPs such as those expressed from FACs. However, *A. nidulans* contains over 70 BGCs (*16*), suggesting that many new compounds still remain to be identified in this fungus. As a twist in the use of FAC technology, here we present a new utility of this technology to induce new endogenous NPs in the expression host. By expressing a *Pseudogymnoascus destructans* squalene synthase (SqsA) containing FAC in *A. nidulans*, we were able to induce biosynthesis of novel endogenous NPs in this host. Instead of producing *P. destructans*–derived metabolites, expression of *sqsA* in *A. nidulans* served as a terpene-regulating tool amplifying and redirecting host-derived meroterpenoid pathways. *A. nidulans* contains two known meroterpenoid BGCs encoding the dominant austinol family (*8*) and the silent aspernidine family (*17*) of metabolites. Heterologous expression of *P. destructans sqsA* FAC redirects the *A. nidulans* biosynthetic output from austinol synthesis to aspernidine synthesis concomitant with the production of three new and six known compounds, four having immunomodulatory properties (Fig. 1). We suggest leveraging *P. destructans sqsA* FAC as a new tool to increase pools of fungal meroterpenoids and a new method to investigate unidentified fungal meroterpenoids such as nidulenes A to E (**1**–**5**).

## RESULTS

### A *P. destructans* FAC induces squalene production in *A. nidulans*

During our search for novel bioactive compounds generated from the FAC transformation of *A. nidulans*, we identified a FAC, Pd-FAC1, from the fungal bat pathogen *P. destructans* containing the gene VC83_00068 (GenBank no.: XM_024463765.1) encoding a putative squalene synthase gene, *sqsA*, whose encoded product showed 50% identity to *Saccharomyces cerevisiae* SqsA (*18*) and a 61% identity to the *A. nidulans* SqsA (AN10396). Squalene synthase, also known as farnesyl-diphosphate farnesyltransferase, is a

[1]Department of Medical Microbiology and Immunology, University of Wisconsin–Madison, Madison, WI, USA. [2]Vaccine and Infectious Disease Division, Fred Hutchinson Cancer Center, Seattle, WA, USA. [3]Department of Chemistry, Northwestern University, Evanston, IL, USA. [4]Intact Genomics Inc., St. Louis, MO, USA. [5]Department of Plant Pathology, University of Wisconsin–Madison, Madison, WI, USA.
*Corresponding author. Email: jwbok@wisc.edu (J.W.B.); npkeller@wisc.edu (N.P.K.)

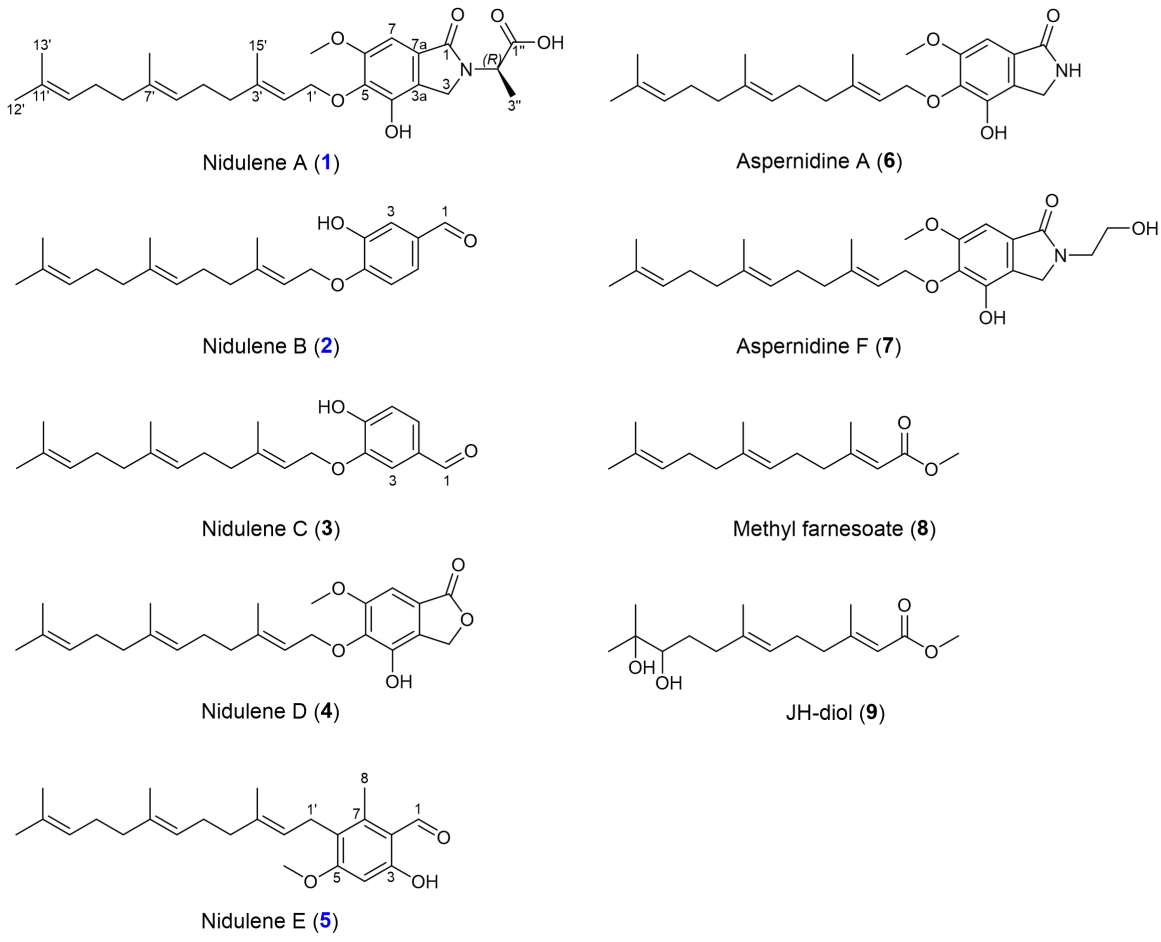


**Fig. 1. Structures of compounds (1 to 9).** The structures of isolated terpenes from PdFAC1.

key enzyme in the isoprenoid pathway (*19*) and is required for the synthesis of ergosterol in fungi (*20*) and cholesterol in animals (*21*) (Fig. 2). The primary product of squalene synthase is squalene, which is formed from dimerization of two molecules of farnesyl pyrophosphate (FPP).

To determine whether the *sqsA* gene from *P. destructans* affected production of squalene in *A. nidulans*, we compared the squalene production level of a control strain (TJW167), an *A. nidulans* transformant with a PdFAC1 (TJW336, GenBank no.: OR972369), and an *A. nidulans* transformant with PdFAC1 deleted for *sqsA* (TJW337) (table S1). Metabolite extracts were analyzed by ultra-high pressure liquid chromatography–high resolution MS (UHPLC–MS/MS), and the resulting datasets were compared using the Maven ver.2.0.3 and MZmine ver.3 software, which facilitates comparative analysis of UHPLC–MS/MS data from multiple different strains. The production of squalene was increased 10-fold in TJW336 compared to the control and TJW337, both of which barely produced detectable squalene (Fig. 3). Thus, the squalene synthase gene in PdFAC1 boosted the production level of squalene in *A. nidulans.*

## PdFAC1 redirects host meroterpenoid production

Although the role of squalene as an ergosterol precursor is well known (*22*), recent papers have shown that alternative functions of SqsA and SqsA-like enzymes and subsequent squalene synthesis are involved in induction of terpenoids in plants (*23*, *24*) and bacteria (*25*). We thus hypothesized that *A. nidulans* transformants expressing PdFAC1 could be altered in terpenoid production. To investigate the effect of SqsA on the chemical composition of host strains, a full range of UHPLC–MS/MS spectra of each strain (control TJW167, TJW336 PdFAC1, and TJW337 PdFAC1Δ*sqsA*) were compared (Fig. 4). While the control strain produced austinol, a cyclized sesquiterpene, as a major *A. nidulans* terpene product, the TJW336 instead produced aspernidine-type meroterpenoids with a linear sesquiterpene attached to the aromatic ring (Fig. 4). From the *sqsA* deleted strain (TJW337), austinol was produced again while the production of aspernidine-type meroterpenoids was gone. Normally the wild-type *A. nidulans* strain used in this study does not produce aspernidines, and its BGC was only found by screening a protein kinase mutation library where one mutant (Δ*mpk*) produced aspernidines, allowing for BGC discovery (*17*). Both PdFAC1 and Δ*mpk* are greatly diminished in ability to produce austinol while overproducing aspernidines, suggesting a possible shift in the precursor shunt pathways common to both strains. Previous studies have indicated that austinol is derived from FPP and 3,5-dimethyl orsellic acid (*17*). Here, it appears that SqsA activity directs FPP into high amounts of squalene in TJW336. We hypothesize that this redirection reduces available FPP pools for austinol synthesis and instead increases squalene pools used in synthesis of aspernidine-like

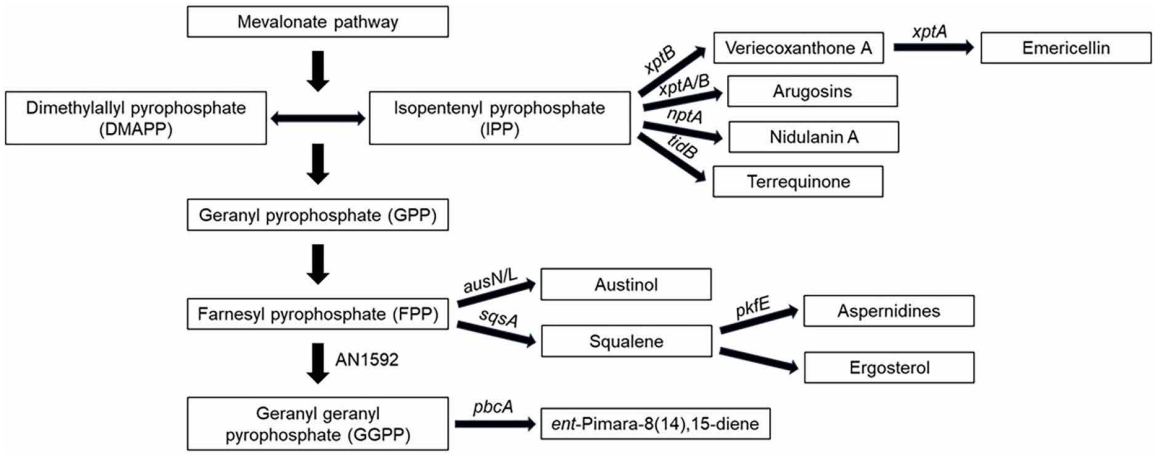


**Fig. 2. The hypothesized scheme of *A. nidulans*–derived terpenes and prenylated metabolites pathways.**

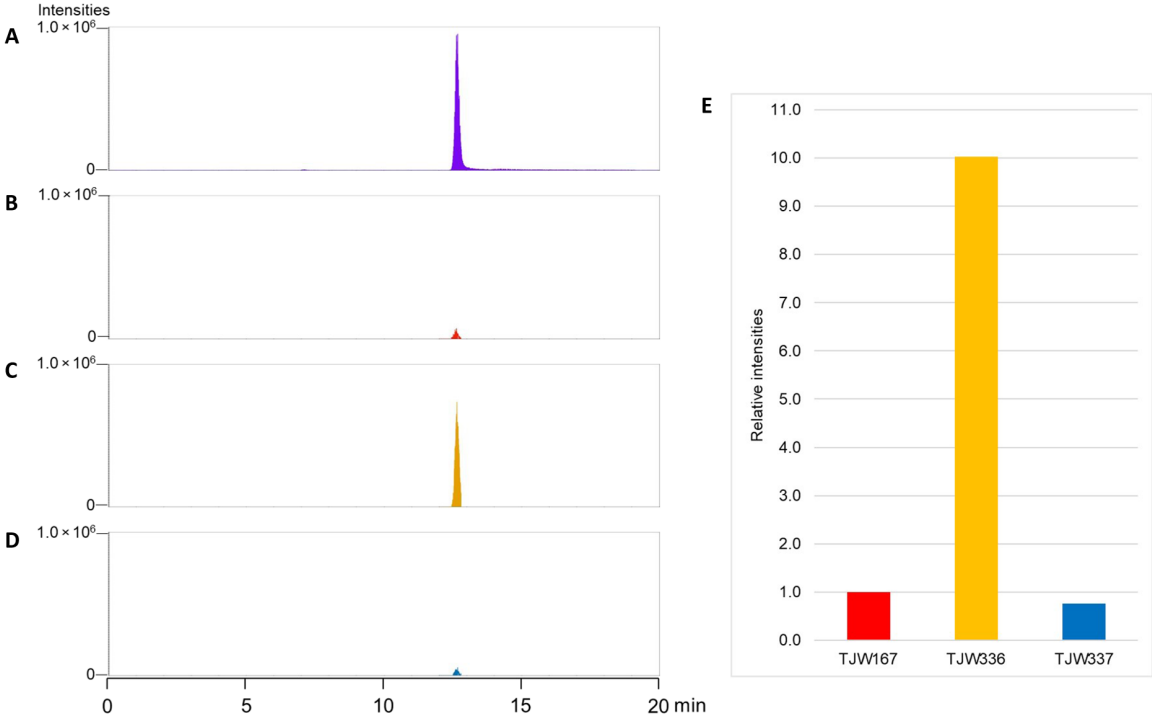


**Fig. 3. Squalene production is dependent on the presence of *P. destructans*–derived squalene synthase gene (*sqsA*).** (**A**) Squalene standard [100 parts per million (ppm)], (**B**) squalene detected from the control strain (TJW167), (**C**) squalene detected from the PdFAC1 transformed *A. nidulans* (TJW336), (**D**) squalene detected from the PdFAC1 transformed *A. nidulans* with deletion of *sqsA* gene (TJW337), and (**E**) relative intensities of squalene production from each strain.

metabolites (Fig. 4). Although it has been speculated that the aspernidine terpene tail is derived from FPP (*26*), our data suggest that squalene could be the source of the farnesyl tail, possibly through degradation through oxygenase activity reminiscent to degradation pathways reported in bacteria (*27*, *28*).

## Structure determination of prenylated compounds isolated from TJW336

To determine the structural analysis of the many terpenoids produced in TJW336, each compound was isolated with HPLC. The molecular formula of compound **1** was deduced to be $C_{27}H_{37}NO_6$ with 10 degrees of unsaturation by high-resolution electrospray ionization MS (HR-ESI-MS) analysis. The $^{13}C$ nuclear magnetic resonance (NMR) spectroscopy and DEPT-135 data of this compound displayed 27 C-atoms, which were assigned to 2 carbonyl carbons ($\delta_C$ 173.8 and 167.3), 12 $sp^2$ carbons ($\delta_C$ 153.8 to 120.8), 6 methyl carbons ($\delta_C$ 55.8 to 15.7), and 7 aliphatic carbons (Table 1). Among the seven aliphatic carbons, four carbons were assigned to methylene carbons ($\delta_C$ 38.9, 38.8, 26.2, and 25.9). The carbon and proton chemical shifts indicated the presence of an oxymethylene ($\delta_C/\delta_H$ 68.2/4.46), a nitrogenous methylene ($\delta_C/\delta_H$ 44.5/4.59 and 4.17), and an $sp^3$ methine ($\delta_C/\delta_H$ 51.2/4.49), which bear nitrogen (Tables 1 and 2).

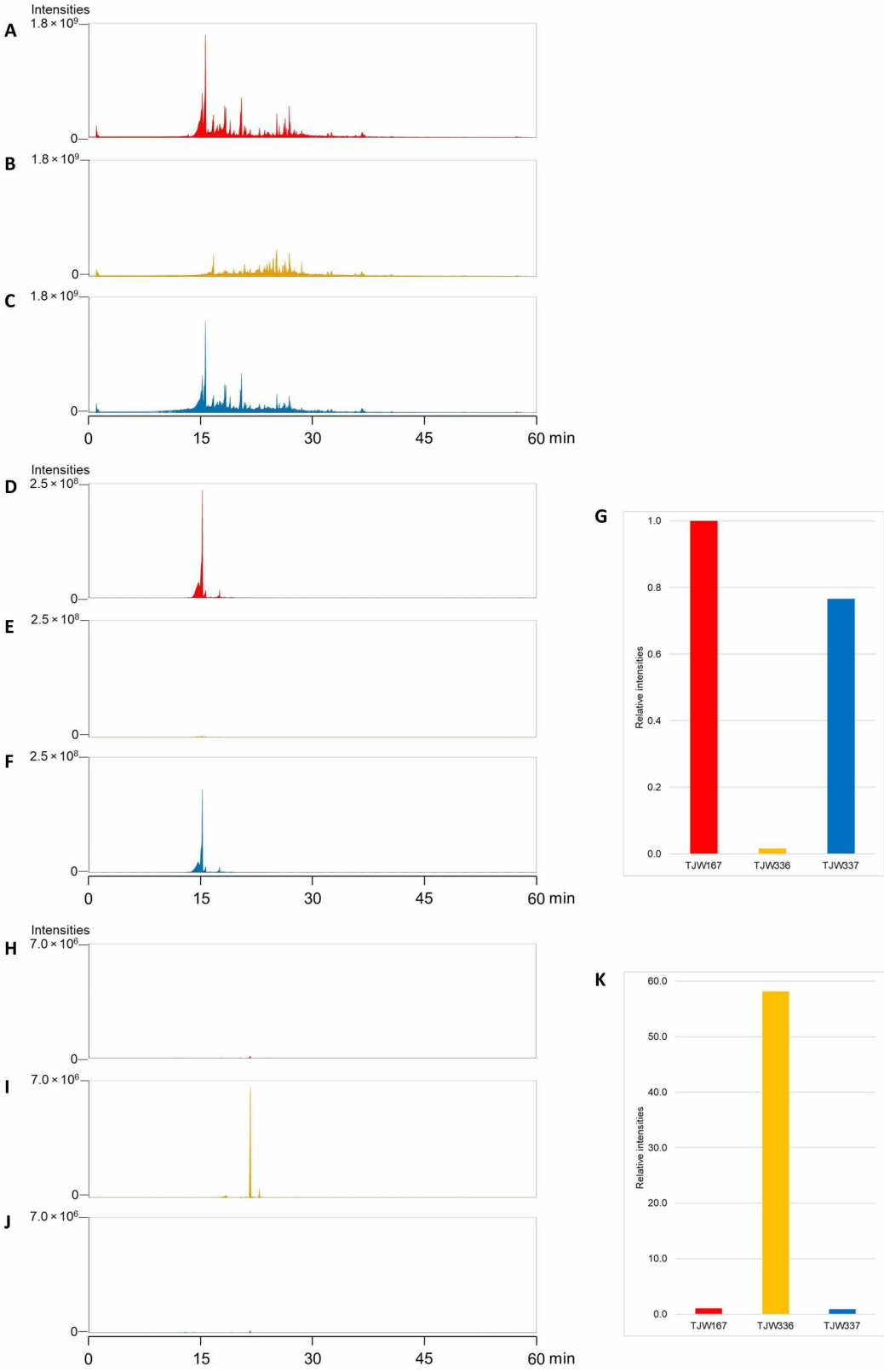


**Fig. 4. Terpene production is dependent on the presence of *P. destructans*–derived squalene synthase gene (*sqsA*).** (**A** to **C**) Full-scan spectra of TJW167 (red), TJW336 (yellow), and TJW337 (blue), respectively. (**D** to **G**) Production of austinol decreased to 2% compared to the control strain and recovered after the deletion of *sqsA*. Austinol ($[M + H]^+ = 459.2006$) was detected at 15.74 min. (**H** to **K**) Production of aspernidine A increased to 58-fold compared to the control strain and dropped to the same level with the control strain after the deletion of *sqsA*. Aspernidine A ($[M + H]^+ = 400.2482$) was detected at 22.42 min.

**Table 1. $^{13}$C NMR (ppm) assignments for compounds 1 to 5.**

| Position | 1* | 2† | 3† | 4† | 5‡ |
|---|---|---|---|---|---|
| 1 | 167.3 | 191.2 | 191.1 | 171.5 | 192.6 |
| 2 | | 130.7 | 130.0 | | 117.4 |
| 3 | 44.5 | 114.2 | 110.1 | 67.6 | 163.5 |
| 3a | 122.4 | | | 121.4 | |
| 4 | 146.7 | 146.5 | 146.6 | 144.9 | 97.0 |
| 5 | 137.6 | 151.3 | 152.1 | 139.0 | 165.5 |
| 6 | 153.8 | 111.4 | 114.5 | 154.3 | 125.6 |
| 7 | 96.5 | 124.6 | 127.6 | 100.0 | 135.3 |
| 7a | 128.2 | | | 126.0 | |
| 8 | | | | | 16.9 |
| 1′ | 68.2 | 66.2 | 66.2 | 69.9 | 25.1 |
| 2′ | 120.8 | 118.3 | 118.4 | 119.0 | 122.4 |
| 3′ | 139.7 | 143.3 | 143.2 | 144.4 | 143.3 |
| 4′ | 38.8 | 39.9 | 39.9 | 39.8 | 40.9 |
| 5′ | 25.9 | 26.3 | 26.3 | 26.4 | 27.3 |
| 6′ | 123.7 | 123.6 | 123.6 | 123.6 | 124.5 |
| 7′ | 134.5 | 135.9 | 135.8 | 135.9 | 136.0 |
| 8′ | 38.9 | 39.7 | 39.7 | 39.9 | 40.8 |
| 9′ | 26.2 | 26.9 | 26.9 | 26.9 | 27.9 |
| 10′ | 124.1 | 124.4 | 124.4 | 124.4 | 125.3 |
| 11′ | 130.6 | 131.6 | 131.6 | 131.6 | 132.1 |
| 12′ | 25.5 | 25.9 | 25.9 | 25.9 | 26.0 |
| 13′ | 17.5 | 17.9 | 17.9 | 17.9 | 17.8 |
| 14′ | 15.7 | 16.2 | 16.2 | 16.2 | 16.3 |
| 15′ | 16.1 | 17.0 | 16.9 | 16.6 | 16.4 |
| 1″ | 173.8 | | | | |
| 2″ | 51.2 | | | | |
| 3″ | 17.2 | | | | |
| 5-OMe | | | | | 56.2 |
| 6-OMe | 55.8 | | | 56.5 | |

*Data were obtained from DMSO-$d_6$. †Data were obtained from $CDCl_3$. ‡Data were obtained from MeOD-$d_4$.

Overall, **1** was found to have two rings based on the combinational analysis of the NMR data (figs. S1 to S6) and the degrees of unsaturation inherent in the mass data, implying that this compound belongs to the prenylated isoindolinone class.

The correlation spectroscopy (COSY) and heteronuclear multiple-bond correlation (HMBC) revealed the characteristic connections within the farnesyl side chain (Fig. 5). The COSY signals of $H_2$-1′–H-2′ ($\delta_H$ 4.46 and 5.48), $H_2$-4′–H-6′ ($\delta_H$ 1.97, 2.02, and 5.08), and $H_2$-8′–H-10′ ($\delta_H$ 1.93, 2.00, and 5.06) and the HMBC correlations of these protons and four methyl protons at $\delta_H$ 1.63, 1.55, 1.55, and 1.59 ($H_3$-12′–$H_3$-15′, respectively) with neighboring carbons revealed the presence of the farnesyl side chain. The HMBC coupling of the methylene protons $H_2$-1′ ($\delta_H$ 4.46) to a quaternary carbon at $\delta_C$ 137.6 indicated *O*-prenylation of the aromatic system. HMBC couplings of $H_2$-3 ($\delta_H$ 4.59 and 4.17) with C-1 ($\delta_C$ 167.3), C-3a ($\delta_C$ 122.4), C-4 ($\delta_C$ 146.7), and C-7a ($\delta_C$ 128.2) and H-7 ($\delta_H$ 6.99) with C-1 ($\delta_C$ 167.3), C-3a ($\delta_C$ 122.4), and C-5 ($\delta_C$ 137.6) revealed the isoindolinone substructure. HMBC coupling of $\delta_H$ 3.90 and C-6 ($\delta_C$ 156.0) established the position of the methoxy substituent. The COSY correlations of H-2″ ($\delta_H$ 4.49) and $H_3$-3″ ($\delta_H$ 1.31) and the HMBC correlations of these protons with C-1″ ($\delta_C$ 173.8) revealed the alanine moiety. The direct linkage between alanine moiety to the isoindolinone moiety was suggested by a crucial HMBC correlation of α-proton of alanine at H-2″ ($\delta_H$ 4.49) and a nitrogenous methylene carbon of isoindolinone at C-3 ($\delta_C$ 44.5). The planar structure of **1** was found to be similar to aspernidine A, a recently reported prenylated isoindolinone from the fungus *A. nidulans*. Thus, compound **1**, designated nidulene A, was determined to be a new aspernidine-type prenylated isoindolinone attached with an alanine.

To determine the absolute configuration at C-2″ of **1**, a comparison of the experimental and calculated electronic circular dichroism (ECD) spectra was carried out. Initially, the calculated ECD results of (*R*)-nidulene A and (*S*)-nidulene A did not show the opposite signs possibly due to the presence of different number of conformers. Total three conformers were obtained from (*R*)-nidulene A, while nine conformers were obtained from (*S*)-nidulene A based on a

**Table 2. $^1$H NMR [δ, mult, (*J* in Hz)] assignments for compounds 1 to 5.**

| Position | 1* | | | 2† | | | 3† | | | 4† | | | 5‡ | |
|---|---|---|---|---|---|---|---|---|---|---|---|---|---|---|
| 1 | | | | 9.84 | s | | 9.82 | s | | | | | 10.36 | s |
| 3 | 4.59 | d | 17.3 | 7.44 | d | 2.0 | 7.43 | s | | 5.22 | s | | | |
| | 4.17 | d | 17.3 | | | | | | | | | | | |
| 4 | | | | | | | | | | | | | 6.38 | s |
| 6 | | | | 6.97 | d | 8.5 | 7.04 | d | 8.0 | | | | | |
| 7 | 6.69 | s | | 7.41 | dd | 8.0, 2.0 | 7.41 | dd | 8.0, 1.5 | 7.01 | s | | | |
| 8 | | | | | | | | | | | | | 2.47 | s |
| 1′ | 4.46 | d | 6.9 | 4.70 | d | 6.0 | 4.68 | d | 6.5 | 4.71 | d | 7.5 | 3.33 | m |
| 2′ | 5.48 | t | 7.0 | 5.49 | t | 7.5 | 5.49 | t | 6.5 | 5.48 | t | 7.0 | 5.03 | m |
| 4′ | 1.97 | dt | 8.2, 6.5 | 1.98 | m | | 1.97 | m | | 1.98 | m | | 1.88 | m |
| 5′ | 2.02 | m | | 2.14 | m | | 2.14 | m | | 2.05 | m | | 2.07 | m |
| 6′ | 5.08 | m | | 5.08 | dt | 6.5 | 5.10 | dt | 6.5 | 5.08 | m | | 5.03 | m |
| 8′ | 1.93 | dt | 8.3, 6.9 | 2.13 | m | | 2.12 | m | | 2.06 | m | | 1.99 | m |
| 9′ | 2.00 | m | | 2.05 | m | | 2.05 | m | | 2.05 | m | | 1.94 | m |
| 10′ | 5.06 | m | | 5.10 | dt | 6.5 | 5.10 | dt | 6.5 | 5.07 | m | | 4.99 | m |
| 12′ | 1.63 | s | | 1.68 | s | | 1.68 | s | | 1.68 | s | | 1.64 | s |
| 13′ | 1.55 | s | | 1.60 | s | | 1.60 | s | | 1.59 | s | | 1.55 | s |
| 14′ | 1.55 | s | | 1.61 | s | | 1.61 | s | | 1.66 | s | | 1.55 | s |
| 15′ | 1.59 | s | | 1.77 | s | | 1.76 | s | | 1.60 | s | | 1.76 | s |
| 1″ | | | | | | | | | | | | | | |
| 2″ | 4.49 | d | 7.3 | | | | | | | | | | | |
| 3″ | 1.31 | d | 7.1 | | | | | | | | | | | |
| 5-OMe | | | | | | | | | | | | | 3.84 | s |
| 6-OMe | 3.79 | s | | | | | | | | 3.93 | s | | | |

*Data were obtained from DMSO-$d_6$. †Data were obtained from $CDCl_3$. ‡Data were obtained from MeOD-$d_4$.

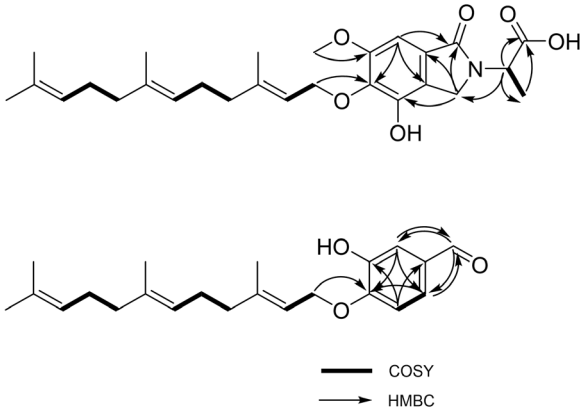


**Fig. 5. Key correlations of COSY (bold) and HMBC (arrows) experiments for compounds 1 and 2.**

density functional theory (DFT)–based computation. As shown in Fig. 6, the experimental CD data of **1** were almost identical to ECD spectrum of (*R*)-nidulene A. Thus, the absolute configuration at C-2″ was assigned to *R* configuration, and the structural similarity with an amino acid alanine suggests that the amino acid side chain of **1** could be derived from D-alanine.

Compound **2** was isolated as a yellow amorphous solid with a formula of $C_{22}H_{30}O_3$ based on HR-ESI-MS analysis. The $^{13}$C NMR data of this compound displayed 22 C-atoms, which were assigned to 1 aldehyde carbon ($\delta_C$ 192.2), 12 $sp^2$ carbons ($\delta_C$ 151.3–111.4), 4 methyl carbons ($\delta_C$ 25.9–16.2), and 5 aliphatic carbons ($\delta_C$ 66.2–26.3) (Table 1 and figs. S7 to S11). Same as compound **1**, the COSY

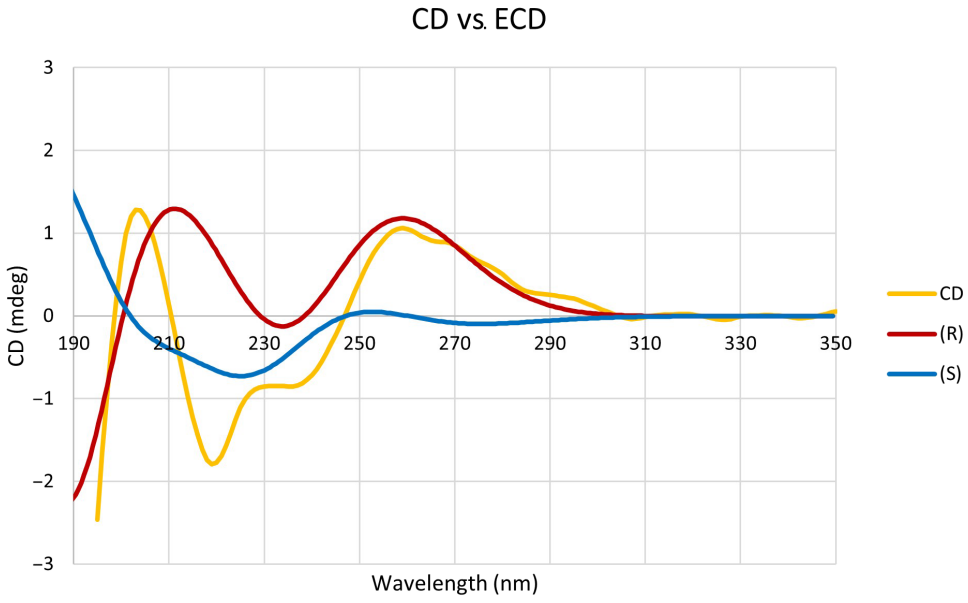


**Fig. 6. Experimental CD spectrum of nidulene A (1) and calculated ECD spectra of (*R*) and (*S*) forms of nidulene A (1).**

and HMBC correlations revealed the farnesyl side chain with 15 C-atoms. Among the remaining seven unassigned carbon atoms, six $sp^2$ carbons ($\delta_C$ 130.7, 114.2, 146.5, 151.3, 114.2, and 124.6; C-2 to C-7, respectively) revealed an aromatic ring based on the combination of COSY and HMBC data (Fig. 5). The HMBC correlations from H-1 ($\delta_H$ 9.84) to C-3 ($\delta_C$ 114.2) and C-7 ($\delta_C$ 124.6) showed the evidence of direct attachment at C-2 position of the aromatic ring. The aromatic ring was constructed by the COSY signal between H-6 ($\delta_H$ 6.97) and H-7 ($\delta_H$ 7.41) with a coupling constant of 8.0 to 8.5 Hz and the HMBC correlations from H-6 ($\delta_H$ 6.97) to C-2 ($\delta_C$ 130.7) and C-4 ($\delta_C$ 146.5), H-7 ($\delta_H$ 7.41) to C-5 ($\delta_C$ 151.3), and H-3 ($\delta_H$ 7.44) to C-5 ($\delta_C$ 151.3) and C-7 ($\delta_C$ 127.6). The HMBC coupling of the methylene protons $H_2$-1′ ($\delta_H$ 4.70) to a quaternary carbon at C-5 ($\delta_C$ 151.3) indicated *O*-prenylation of the aromatic ring. Thus, compound **2**, designated nidulene B, was determined to be a new asperugin-type prenylated aromatic derivative.

The $^{13}C$ and $^{1}H$ NMR data (figs. S12 and S13) of compound **3**, which is a known compound (*29*) and has the same molecular formula with **2**, were similar to those obtained for **2**. Both compounds **2** and **3** had the identical carbon and proton chemical shifts for the structure of the farnesyl side chain. The most noticeable difference between **2** and **3** was the replacement of the attachment of a farnesyl chain. For compound **2**, the terpene tail was attached to the *para* position, while compound **3** has a tail at the *meta* position of the aromatic system. Compound **3** was a known compound without proper name (*29*). Thus, compound **3** was named as nidulene C.

The molecular formula of **5** was established as $C_{24}H_{34}O_3$ by HR-ESI-MS analysis. On the basis of a combination of spectroscopic analyses and a literature survey, compound **5** was identified as a methoxy adduct of the ovinal (figs S16 and S17) (*30*). Although the spectroscopic data of this compound were reminiscent of those of **1** to **4**, several differences were found in the structure of **5**. First, it was found that there is no oxygen bridge between the farnesyl tail and the aromatic head. In addition, there was one extra methyl group in the aromatic system than **1** to **4**. Unlike the other four compounds, compound **5** had a direct attachment of methyl to the aromatic head. The planar structure of the compound is the same as ovinal, isolated from *Albatrellus ovinus*, with an extra methoxy group. Thus, the structure of **5**, designated nidulene E, was determined to be a new ovinal derivative (*30*).

In addition to **1** to **3** and **5**, five known compounds, prenylated isoindolinone alkaloids (**5**, **6**, and **7**), and linear sesquiterpenes (**8** and **9**) were also isolated. On the basis of a combination of spectroscopic analyses and literature investigations (figs. S14, S15, and S18 to S25); these compounds were identified as an aspernidine derivative (**5**) (*29*), aspernidine A (**6**) (*26*), aspernidine F (**7**) (*31*), methyl farnesoate (**8**) (*32*), and JH-diol (**9**) (*33*). The spectroscopic data of these compounds were in good agreement with the reported values. Among these compounds, **4** had not been previously named; therefore, it was named as nidulene D (*29*).

## Human neutrophil chemotaxis is induced by nidulene E (3) and inhibited by nidulene A (1), nidulene C (4), and aspernidine F (7)

As a preliminary examination of crude extracts from TJW336 showed impacts on neutrophil mobility and several studies have identified chemotactic properties of other terpenoids (*34*, *35*), we examined all purified metabolites for any effects on neutrophil migration. Upon screening all compounds, nidulene E (**3**) was the only chemoattractive compound. In comparison to the vehicle control [dimethyl sulfoxide (DMSO)], we saw increased neutrophil movement to concentrations 0.1, 1.0, 10, and 100 μg/ml of nidulene E (**3**) ($P = 0.0134$, 0.0081, and <0.0001, respectively). Nidulene E (**3**) at 100 μg/ml showed the greatest impact on neutrophil chemotaxis, though less than our positive control *N*-formylmethionyl-leucyl-phenylalanine (*f*MLP) ($P < 0.0001$) (Fig. 7A). Inhibition of *f*MLP-driven neutrophil chemotaxis occurred with the following compounds: nidulene A (**1**) (100 μg/ml, $P = 0.0009$), nidulene C (**4**) (100 μg/ml, $P = 0.0222$), and aspernidine F (**7**) (100 μg/ml, $P = 0.0001$) (Fig. 7, B to D). Compounds **2**, **4**, **8**, and **9** resulted in no chemotaxis or inhibition of

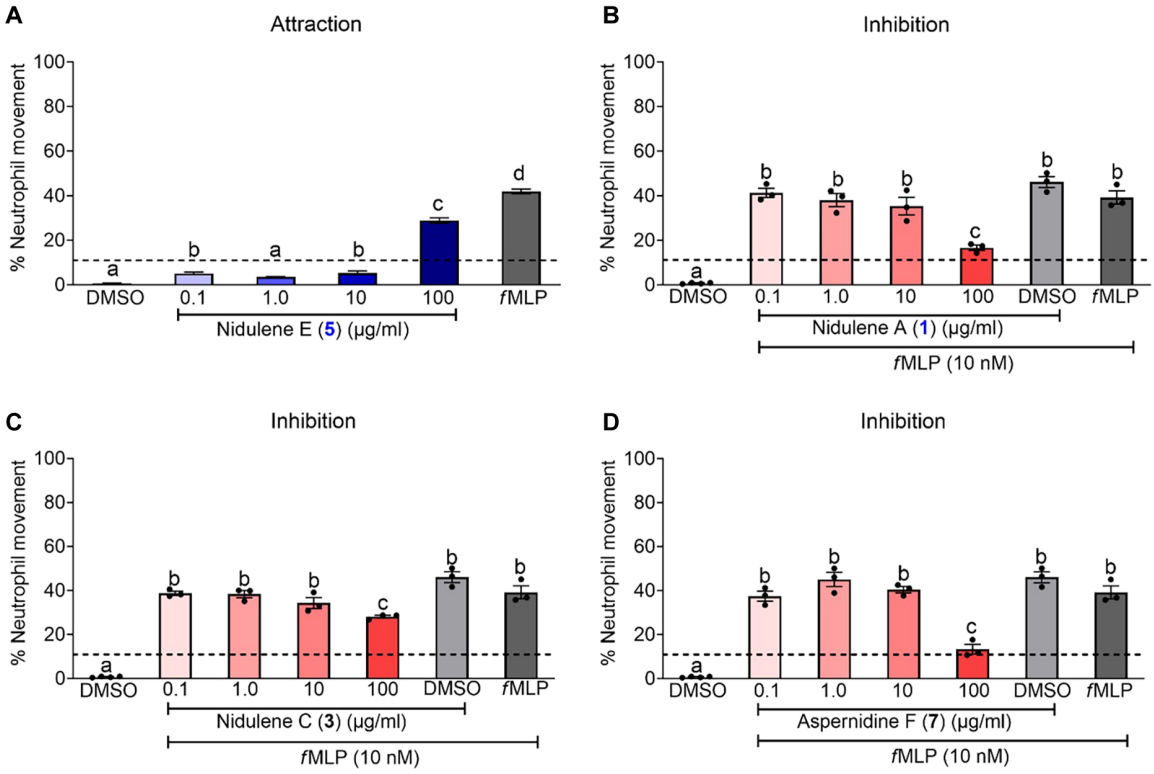


**Fig. 7. Neutrophil movement is affected by compounds 1, 3, 5, and 7.** (**A**) Nidulene E (**3**) is a chemoattractant for human neutrophils. Using a Boyden chamber, neutrophils stained with calcein AM were seeded in the upper chamber at $5 \times 10^4$ cells per well and incubated at 37°C for 1 hour with the vehicle (DMSO; light gray bar), positive control (*f*MLP, 10 nM; dark gray bar), or nidulene E (**3**) at four different concentrations (0.1, 1.0, 10, or 100 μg/ml; blue bars) found in the lower chamber. The media control is indicated as a dotted line across the graph. (**B** to **D**) Inhibition of *f*MLP-driven neutrophil chemotaxis by nidulene A (**1**), nidulene C (**4**), and aspernidine F (**7**). As described above, neutrophils stained with calcein AM were seeded in the upper chamber at $5 \times 10^4$ cells per well and incubated at 37°C for 1 hour with the vehicle (DMSO, light gray bar), the DMSO vehicle with *f*MLP (*f*MLP at 10 nM; medium gray bar), positive control (*f*MLP, 10 nM; dark gray bar), or the respective compounds at four different concentrations (0.1, 1.0, 10, or 100 μg/ml; red bars) found in the lower chamber. The media control is indicated as a dotted line across the graph. For all graphs (A to D), cells that migrated into the lower chamber were quantified using flow cytometry and the percent live cells that migrated were determined by calculating the percent live neutrophils from the loading control. Samples are listed as average ± SEM, and assays have been repeated to assure reproducibility. Statistical differences were assessed using one-way analysis of variance (ANOVA). Different letters denote statistical differences.

chemotaxis across the concentrations tested (figs. S26 and S27). Aspernidine A (**6**) was tested for both chemotaxis and inhibition, but the data were inconclusive because of its high toxicity (data not shown).

## DISCUSSION

The activation of silent gene clusters in fungi for production of uncharacterized secondary metabolites has garnered substantial attention in recent years (*36*). Genetic tools play a crucial role in this pursuit by providing means to unlock the hidden potential of fungal genomes (*37*). One such tool is the implementation of FAC technology that can specifically target and activate silent BGCs in heterologous hosts (*10*). By applying FAC method inversely, we present a twist to FAC utility where we demonstrate that heterologous expression of a *P. destructans* FAC containing a squalene synthase induced cryptic *A. nidulans* aspernidine family compounds including uncharacterized novel immunomodulatory compounds (**1**, **2**, and **5**; Fig. 1). This activation of aspernidines was accompanied by near loss of austinol, which is considered the primary terpene product in *A. nidulans* (Figs. 2 and 4). The shift of the terpene profile was correlated with shunting of FPP into squalene, thus presenting the potential of terpene manipulation via overexpression of primary metabolite enzymes to redirect flow of the isoprene precursor to different products.

Both FPP and squalene are incorporated into numerous terpenes. Canonical classes include sesquiterpenoids derived from the FPP precursor and triterpenoids derived from squalene (*38*, *39*). Logic based on aspernidine structure, therefore, suggested that the linear tail was derived from FPP, but our results suggest that the sesquiterpene tail is more likely derived from the triterpene squalene (Fig. 2). Traditionally, terpenes were categorized by the number of isoprenyl units they contained and the origin of terpenes was assumed on the basis of the linear form of isoprenyl units (*40*). However, more recent studies have characterized a variety of terpenes that do not follow the traditional isoprenyl unit rational. For example, triterpenes talaropentaene, macrophomene, and colleterpenol are identified as nonsqualene triterpene compounds (*41*). Oxidative degradation of squalene into smaller terpenes has been reported in several publications (*27*, *28*, *42*). Our work also supports a noncanonical incorporation of squalene into a sesquiterpenoid containing family of metabolites.

The terpenoid potential of *A. nidulans* is only partially defined. Of the ~35 terpene synthesis–related genes including terpene synthases, terpene cyclases, and/or prenyl transferases, found in the sequenced *A. nidulans* FGSC A4 genome (the isolate used in this study), only 9 have been genetically linked to their product: AN1592 and AN1594 (PbcA) to *ent*-pimara-8(14),15-diene, AN9259 (AusN) and AN9257 (AusL) to austinol, AN3228 (PkfE) to aspernidines, AN8514 (tidB) to terrequinone, AN11080 (nptA) to nidulanin A, and AN6784 (xptA) and AN12402 (xptB) to prenylated xanthones (Fig. 2). Products of AN3252, AN6810, and AN9314 are yet to be determined (*43*). Further, there is variation in the genomes of different *A. nidulans* isolates where, for example, isolate SP260548 is missing the austinol clusters (*16*). The results of this study suggest a close relationship between the production of two different *A. nidulans*–derived sesquiterpenes, austinol and aspernidines, and also implicate the involvement of squalene in the synthesis of aspernidine. By manipulating genes in the host strain, we can gain insights into the correlations of host-derived terpenes and their biosynthetic pathways. Gene manipulation has been instrumental in elucidating terpene discovery in fungi, allowing researchers to gain a deeper understanding of the biosynthetic pathways and regulation of terpene production. For instance, the biosynthetic pathway of the fungal meroterpenoid anditomin, along with its precursors, was clearly identified by heterologous expression of related BGCs from *Aspergillus variecolor* in *Aspergillus oryzae* (*44*). Moreover, by manipulating potential terpene cyclases in the host strain *Fusarium fujikuroi*, researchers successfully produced and isolated new fungal terpenes, koraiol, and α-acorenol (*45*).

The biological activities of aspernidines are not well characterized, with only two studies to date demonstrating moderate antiproliferative activities of aspernidines A and B (*26*) and antitumor properties of aspernidine H in A-594 and SW-480 cell lines (*31*). On the basis of initial activities of crude extracts of TJW336, we focused on examining any impact of the nine purified compounds on neutrophil migration. The human neutrophil chemotaxis results supported this initial observation and presented a first look into structure activity relationships of these compounds (table S2). The aromatic head of these compounds can have immense structural variations, such as isoindolinone, phthalimidine, and phenol, and we found most differences in bioactivities attributable to these structural distinctions. Nidulene A (**1**), nidulene C (**4**), and aspernidine F (**7**) inhibited neutrophil chemotaxis, whereas nidulene E (**3**) promoted migration. On the basis of the structural differences matched with the neutrophil migration results, there are several clues that may explain where the activity comes from. For example, nidulene A (**1**), aspernidine A (**6**), and aspernidine F (**7**) shared the same moiety, which is an isoindolinone but showed different activity. The additional functional groups on the nitrogen from the isoindolinone moiety (compounds **1** and **7**) may present inhibition activity toward human neutrophil cells, while an NH-proton of the same moiety (compound **6**) may present the cytotoxicity. Unlike other isolated meroterpenes, nidulene E (**3**) showed some chemotaxis activity possibly caused by either the different aromatic head moiety or direct attachment of a linear terpene to the aromatic system without an oxygen bridge. Since the differences from the aromatic head of each terpene showed different activities, we hypothesized that the aromatic head of the terpene may differentiate the inhibition activity on human neutrophil cells.

In conclusion, a tool that shifts the flux of precursors into multiple SM biosynthetic pathways and induces production of novel cryptic compounds has substantial potential to drive discovery of novel bioactive compounds. Terpenes encompass a broad class of natural compounds that hold substantial promise for therapeutic applications (*46*, *47*). Gaining mastery over the biosynthesis of fungal terpenes opens up new avenues in drug development. Thus, developing methods of controlling and/or altering the production of various terpenes in fungal strains through terpene gene manipulation will add to our understanding of the biosynthetic pathway and biological role of fungal terpenoids (*48*). In this research, we took a different approach using FAC and demonstrated that when a PdFAC1 including *sqsA* was expressed heterologously in *A. nidulans*, it led to changes in the host biosynthesis of endogenous terpene pathways. Compared to the control strain (TJW167), the PdFAC1 transformant (TJW336) exhibited increased production of squalene and compounds belonging to the aspernidine family. We identified three novel and six known fungal terpenes (**1**–**9**). We propose a mechanism in which the conversion of FPP to squalene by *sqsA* leads to increased synthesis of aspernidine-type compounds, which may be derived from the squalene at the expense of FPP-derived austinol. We speculate that this method could be used to successfully modify terpene profiles in other fungi. This research highlights the potential utility of FACs in altering fungal metabolite production and sheds light on the interplay between terpene biosynthetic pathways in filamentous fungi.

## MATERIALS AND METHODS

### *P. destructans* FAC library

The fungal strains (table S1) used in this study are *A. nidulans* RJW256 and *P. destructans* 20631-21. *A. nidulans* RJW256 is used as the heterologous host for FAC transformation. For the high molecular weight (HMW) genomic DNA isolation and FAC library construction, *P. destructans* was inoculated from a concentrated spore stock in liquid glucose minimal media (GMM) (*49*). Cultures were incubated at 15°C for 2 days, and HMW genomic DNA was prepared and FAC library was constructed according to the method described previously (*10*). All FAC clones and FAC library are cloned in *Escherichia coli* strain: igMax DH10B electrocompetent cells.

### PdFAC1 identification, resequencing, and key gene deletion via FAC recombineering

Similar to bacterial artificial chromosome pooling and sequencing (*50*), *P. destructans* FAC library was pooled according to Column_Row_Plate, and their pooled DNAs were sequenced by using dual-indexing Illumina sequencing, DNA assembly, annotation, BGC prediction, and BGC-containing FAC identification with an in-house bioinformatics pipeline. PdFAC1 contained the gene VC83_00068 (GenBank no.: XM_024463765.1) encoding a putative squalene synthase, SqsA. *sqsA* was deleted in PdFAC1 using a pair of primers (table S3) to create the FAC deletant: TJW337 via *E. coli* SW101 using Red/ET tools as previously mentioned (table S3) (*51*, *52*). PdFAC1 was confirmed by resequencing and reannotated.

### Transformation of FACs into the heterologous host strain and construction of TJW336 and TJW337

Transformation in *A. nidulans* was followed as described in a previous study (*53*). Briefly, 0.2 μg of FAC DNA was mixed with protoplasts ($10^7$ protoplasts/ml) in the presence of 30% polyethylene glycol 4000 (PEG-4000) with 50 mM $CaCl_2$ for fungal transformation, and

transformed protoplast was regenerated on solid GMM with 1.2 M sorbitol and pyridoxine (1 ml of a 0.1% stock solution) as a supplement and incubated for 3 days at 37°C in an incubator to obtain transformants. All transformants were confirmed by polymerase chain reaction (PCR) using a pair of primer listed in table S3 (data not shown). We constructed the fungal heterologous expression strains: *A. nidulans*/PdFAC1 as TJW336 and *A. nidulans*/PdFAC1Δ*sqsA* as TJW337, respectively.

### Fungal culture and extraction of secondary metabolites

The control strain TJW167, TJW336, and TJW337 were inoculated on triplicated GMM plates with small amount of agar plug scraped off of the plates using sterile toothpick and incubated for 7 days at 37°C as previously reported (*11*). Subsequently, the entire contents of the plates were collected and lyophilized for 48 hours. Samples were then pulverized with a mortar and pestle, and methanol was added. Air-dried methanol extracts were prepared with a SpeedVac system (Savant SpeedVac Concentrator, SC250EXP-115) and then further extracted with organic solvent (chloroform:methanol:ethylacetate, 8:1:1). Organic extracts were evaporated to dryness in a SpeedVac and stored at −20°C until analysis. For the metabolite isolation and purification, 15 g of crude extract of TJW336 was obtained from 600 plates of solid GMM incubated for 7 days at 37°C.

### UHPLC–HRMS/MS analysis

UHPLC-HRMS data were acquired using a Thermo Fisher Scientific Q Exactive Orbitrap mass spectrometer (Waltham, MA, USA) coupled to a Vanquish UHPLC (Waltham, MA, USA) operated in positive ionization mode. All solvents used were of spectroscopic grade. Extracts from the conditions described below were diluted into 1 mg/ml and used as samples for UHPLC–HRMS/MS. For the general screening including terpenes, a Waters XBridge BEH-C18 column (2.1 mm × 100 mm, 1.7 μm) was used with acetonitrile (0.05% formic acid) and water (0.05% formic acid) as solvents at a flow rate of 0.2 ml/min. The screening gradient method for the samples is as follows: Starting at 10% organic for 5 min, followed by a linear increase to 90% organic over 20 min, another linear increase to 98% organic for 2 min, holding at 98% organic for 5 min, decreasing back to 10% organic for 3 min, and holding at 10% organic for the final 2 min, for a total of 37 min. For the squalene detection, the same Waters XBridge BEH-C18 column (2.1 mm × 100 mm, 1.7 μm) was used with methanol and water as solvents at a flow rate of 0.2 ml/min. The screening gradient method for the samples is as follows: Starting at 75% organic followed by a linear increase to 98% organic over 2 min, holding at 98% organic for 15 min, decreasing back to 75% organic for 0.2 min, and holding at 75% organic for the final 2.8 min, for a total of 20 min. A quantity of 10 μl of each sample was injected into the system for the analysis. Each extract was diluted in 1 mg/ml in methanol, and 100 parts per million (ppm) of squalene was used as standard.

### General experimental procedures

Ultraviolet (UV) spectra were acquired using a Cary Bio400 UV/Vis spectrophotometer (Varian Inc., Palo Alto, CA, USA). CD spectra were recorded on an AVIV model 420 circular dichroism spectrometer (Hod Hasharon, Israel). Infrared (IR) spectra were recorded on a JASCO 4200 FT-IR spectrometer (Easton, MD, USA) using a ZnSe cell. NMR spectra were recorded in MeOD-$d_4$, DMSO-$d_6$, or $CDCl_3$ solutions on Bruker Avance III HD, 500 MHz instrument (Billerica, MA, USA) equipped with a 5-mm cryoprobe. NMR spectra were processed and baseline-corrected using MestReNova software. UHPLC-HRMS and UHPLC–MS/MS data were acquired using a Thermo Fisher Scientific Vanquish UHPLC system (Waltham, MA, USA) connected to a Thermo Fisher Scientific Q Exactive Hybrid Quadrupole-Orbitrap mass spectrometer (Waltham, MA, USA) operated in positive and/or negative ionization modes using a mass/charge ratio (*m/z*) range of 190 to 2000. HPLC separations were performed on a Gilson 332 pump and a Gilson 171 DAD detector (Middleton, WI, USA). All solvents used were of spectroscopic grade.

### Compound isolation and purification

The terpene-type compounds from half of the crude extract of TJW336 were initially isolated by preparative reversed-phase HPLC (Waters Xbridge PREP C18 OBD column, 5 μm, 19 mm × 250 mm) using a gradient solvent system (50% $CH_3CN$-$H_2O$ to 90% $CH_3CN$-$H_2O$ over 35 min, UV detection at 210 nm, and flow rate = 16 ml/min) and afforded compounds **1** ($t_R$ = 21.8 min), **5** ($t_R$ = 28.4 min), **6** ($t_R$ = 20.2 min), **7** ($t_R$ = 17.3 min), **8** ($t_R$ = 33.3 min), and **9** ($t_R$ = 17.1 min). Another half of the crude extract was loaded onto the same column using a different gradient solvent system (20% $CH_3CN$-$H_2O$ to 95% $CH_3CN$-$H_2O$ over 24 min, UV detection at 210 nm, and flow rate = 16 ml/min). The fifth fraction (51.2 mg) that eluted with 95% $CH_3CN$-$H_2O$ was separated by preparative reversed-phase HPLC (68% $CH_3CN$-$H_2O$ over 30 min, UV detection at 210 nm, and flow rate = 16 ml/min) and afforded compounds **2** ($t_R$ = 24.0 min), **3** ($t_R$ = 26.1 min), and **4** ($t_R$ = 27.5 min). Compound **1** was purified by an analytical HPLC (68% $CH_3CN$-$H_2O$ over 30 min, UV detection at 210 nm, and flow rate = 2.0 ml/min; YMC-ODS-A column, 4.6 mm × 250 mm; $t_R$ = 22.1 min, respectively). The purified metabolites were isolated in the following amounts: 2.3, 5.6, 5.5, 7.7, 7.6, 3.4, 1.5, 4.4, and 3.3 mg of **1** to **9**, respectively.

Nidulene A (**1**): yellow, amorphous solid; UV (MeOH) $\lambda_{max}$ (log ε) 208 (4.24), 263 (1.26) nm; IR (ZnSe) $\nu_{max}$ 3247 (br), 1758, 1671 $cm^{-1}$; $^1H$ and $^{13}C$ NMR data, Tables 1 and 2; HR-ESI-MS *m/z* 472.2684 $[M + H]^+$ (calcd for $C_{27}H_{38}NO_6$, 472.2694).

Nidulene B (**2**): yellow, amorphous solid; UV (MeOH) $\lambda_{max}$ (log ε) 194 (5.84), 229 (2.34), 276 (1.84), 311 (1.45) nm; IR (ZnSe) $\nu_{max}$ 3250 (br), 1734, 1629 $cm^{-1}$; $^1H$ and $^{13}C$ NMR data, Tables 1 and 2; HR-ESI-MS *m/z* 343.2112 $[M + H]^+$ (calcd for $C_{22}H_{31}O_3$, 343.2112).

Nidulene E (**3**): yellow, amorphous solid; UV (MeOH) $\lambda_{max}$ (log ε) 205 (5.39), 265 (1.33) nm; IR (ZnSe) $\nu_{max}$ 3224 (br), 1729, 1608 $cm^{-1}$; $^1H$ and $^{13}C$ NMR data, Tables 1 and 2; HR-ESI-MS *m/z* 371.2572 $[M + H]^+$ (calcd for $C_{24}H_{35}O_3$, 371.2581).

### ECD calculations

The conformational search for the C-2″ position of compound **1** was performed using Spartan 14 (v.1.1.7 Wavefunction Inc., Irvine, CA, USA) to identify all possible conformers for each isomer. Through Gaussian 16 software (Wallingford, CT, USA), the equilibrium geometries were optimized to the ground-state level based on the DFT calculations. The basis parameter set used was B3LYP. Conformers within 15 kJ/mol of each global minimum for *R* and *S* form of **1** were used for gauge-independent atomic orbital shielding constant calculations without geometry optimization at the B3LYP level.

### Human neutrophil chemotaxis to purified compounds (1–9)

Human blood was donated by healthy volunteers based on protocols reviewed and approved by the Institutional Review Board at the

University of Wisconsin-Madison. Using a MACSpress neutrophil isolation kit (no. 130-104-434, Miltenyi) and the erythrocyte depletion kit (no. 130-098-196, Miltenyi), we isolated human neutrophils from whole blood and stained cells with calcein AM (C1430, Thermo Fisher Scientific) at 4°C for 1 hour in the dark. Cells were rinsed with phosphate-buffered saline (PBS) and resuspended to $5 \times 10^5$ cells/ml. Using a previously established protocol (*54*) with some modifications, a transwell plate (96-well) is prepared 24 hours before the assay by incubating the upper and lower wells with fibrinogen (10 μg/ml) for 1 hour at 37°C with gentle shaking. Wells were washed with PBS and blocked with 2% bovine serum albumin for 30 min at 37°C before aspiration and drying overnight. On the day of the assay, compounds were diluted in mHBSS (1× Hanks' balanced salt solution, 0.1% human serum albumin, and 20 mM Hepes) and added to the respective lower wells at 100 μl per well. In addition, vehicle controls and *f*MLP (10 nM) were also prepared in mHBSS and added to requisite wells. Neutrophils were added to the upper chamber at $5 \times 10^4$ cells per well, and a loading control was used to ensure that equal numbers of cells were loaded. Plates were incubated for 1 hour at 37°C. Following incubation, we released cells by adding 45 mM EDTA (pH 8.0) to lower wells for 15 min at 4°C. Samples were transferred to a U-bottom 96-well plate and run on the plate reader of the attune for enumeration following setup of the machine with single-stained samples. The attune was set to mix once before drawing up and reading 120 μl of fluid per well. Data were analyzed using FlowJo (10.8.1) software. Percent cell movement was determined by assessing the number of live cells in the treatment well and dividing by the total number of cells recorded in the loading controls.

## Supplementary Materials

**This PDF file includes:**

Figs. S1 to S27
Tables S1 to S4
References

## REFERENCES AND NOTES


1. N. P. Keller, Fungal secondary metabolism: Regulation, function and drug discovery. *Nat. Rev. Microbiol.* **17**, 167–180 (2019).
2. A. A. Brakhage, Regulation of fungal secondary metabolism. *Nat. Rev. Microbiol.* **11**, 21–32 (2013).
3. S. Sanchez, A. L. Demain, Bioactive products from fungi. *Food Bioact.* 59–87 (2017).
4. Y. Matsuda, I. Abe, Biosynthesis of fungal meroterpenoids. *Nat. Prod. Rep.* **33**, 26–53 (2016).
5. R. Geris, T. J. Simpson, Meroterpenoids produced by fungi. *Nat. Prod. Rep.* **26**, 1063–1094 (2009).
6. M. Nazir, M. Saleem, M. I. Tousif, M. A. Anwar, F. Surup, I. Ali, D. Wang, N. Z. Mamadalieva, E. Alshammari, M. L. Ashour, A. M. Ashour, I. Ahmed, Elizbit, I. R. Green, H. Hussain, Meroterpenoids: A comprehensive update insight on structural diversity and biology. *Biomolecules* **11**, 957 (2021).
7. M. Zhao, Y. Tang, J. Xie, Z. Zhao, H. Cui, Meroterpenoids produced by fungi: Occurrence, structural diversity, biological activities, and their molecular targets. *Eur. J. Med. Chem.* **209**, 112860 (2021).
8. M. Jiang, Z. Wu, L. Liu, S. Chen, The chemistry and biology of fungal meroterpenoids (2009-2019). *Org. Biomol. Chem.* **19**, 1644–1704 (2021).
9. A. A. Brakhage, V. Schroeckh, Fungal secondary metabolites—Strategies to activate silent gene clusters. *Fungal Genet. Biol.* **48**, 15–22 (2011).
10. J. W. Bok, R. Ye, K. D. Clevenger, D. Mead, M. Wagner, A. Krerowicz, J. C. Albright, A. W. Goering, P. M. Thomas, N. L. Kelleher, N. P. Keller, C. C. Wu, Fungal artificial chromosomes for mining of the fungal secondary metabolome. *BMC Genomics* **16**, 343 (2015).
11. K. D. Clevenger, J. W. Bok, R. Ye, G. P. Miley, M. H. Verdan, T. Velk, C. Chen, K. Yang, M. T. Robey, P. Gao, M. Lamprecht, P. M. Thomas, M. N. Islam, J. M. Palmer, C. C. Wu, N. P. Keller, N. L. Kelleher, A scalable platform to identify fungal secondary metabolites and their gene clusters. *Nat. Chem. Biol.* **13**, 895–901 (2017).
12. L. K. Caesar, M. T. Robey, M. Swyers, M. N. Islam, R. Ye, P. P. Vagadia, G. E. Schiltz, P. M. Thomas, C. C. Wu, N. L. Kelleher, N. P. Keller, J. W. Bok, Heterologous expression of the unusual terreazepine biosynthetic gene cluster reveals a promising approach for identifying new chemical scaffolds. *mBio* **11**, e01691-20 (2020).
13. G. Pontecorvo, J. A. Roper, L. M. Hemmons, K. D. Macdonald, A. W. J. Bufton, The genetics of *Aspergillus nidulans*. *Adv. Genet.* **5**, 141–238 (1953).
14. Y.-M. Chiang, T.-S. Lin, C. C. C. Wang, Total heterologous biosynthesis of fungal natural products in *Aspergillus nidulans*. *J. Nat. Prod.* **85**, 2484–2518 (2022).
15. L. K. Caesar, N. L. Kelleher, N. P. Keller, In the fungus where it happens: History and future propelling *Aspergillus nidulans* as the archetype of natural products research. *Fungal Genet. Biol.* **144**, 103477 (2020).
16. M. T. Drott, R. W. Bastos, A. Rokas, L. N. A. Ries, T. Gabaldón, G. H. Goldman, N. P. Keller, C. Greco, Diversity of secondary metabolism in *Aspergillus nidulans* clinical isolates. *mSphere* **5**, e00156-20 (2020).
17. J. Yaegashi, M. B. Praseuth, S.-W. Tyan, J. F. Sanchez, R. Entwistle, Y.-M. Chiang, B. R. Oakley, C. C. C. Wang, Molecular genetic characterization of the biosynthesis cluster of a prenylated isoindolinone alkaloid aspernidine A in *Aspergillus nidulans*. *Org. Lett.* **15**, 2862–2865 (2013).
18. D. Zhang, S. M. Jennings, G. W. Robinson, C. D. Poulter, Yeast squalene synthase: Expression, purification, and characterization of soluble recombinant enzyme. *Arch. Biochem. Biophys.* **304**, 133–143 (1993).
19. H. Y. Chang, T. H. Cheng, A. H. Wang, Structure, catalysis, and inhibition mechanism of prenyltransferase. *IUBMB Life* **73**, 40–63 (2021).
20. M. A. Kennedy, M. Bard, Positive and negative regulation of squalene synthase (ERG9), an ergosterol biosynthetic gene, in Saccharomyces cerevisiae. *Biochim. Biophys. Acta* **1517**, 177–189 (2001).
21. R. Do, R. S. Kiss, D. Gaudet, J. C. Engert, Squalene synthase: A critical enzyme in the cholesterol biosynthesis pathway. *Clin. Genet.* **75**, 19–29 (2009).
22. N. D. Lees, B. Skaggs, D. R. Kirsch, M. Bard, Cloning of the late genes in the ergosterol biosynthetic pathway of *Saccharomyces cerevisiae*—A review. *Lipids* **30**, 221–226 (1995).
23. C. Wen, Z. Zhang, Q. Shi, R. Niu, X. Duan, B. Shen, X. Li, Transcription factors *ZjMYB39* and *ZjMYB4* regulate farnesyl diphosphate synthase- and squalene synthase-mediated triterpenoid biosynthesis in jujube. *J. Agric. Food Chem.* **71**, 4599–4614 (2023).
24. A. Grover, G. Samuel, V. S. Bisaria, D. Sundar, Enhanced withanolide production by overexpression of squalene synthase in Withania somnifera. *J. Biosci. Bioeng.* **115**, 680–685 (2013).
25. R. Nagata, H. Suemune, M. Kobayashi, T. Shinada, K. Shin-Ya, M. Nishiyama, T. Hino, Y. Sato, T. Kuzuyama, S. Nagano, Structural basis for the prenylation reaction of carbazole-containing natural products catalyzed by squalene synthase-like enzymes. *Angew. Chem. Int. Ed. Engl.* **61**, e202117430 (2022).
26. K. Scherlach, J. Schuemann, H.-M. Dahse, C. Hertweck, Aspernidine A and B, prenylated isoindolinone alkaloids from the model fungus *Aspergillus nidulans*. *J. Antibiot. (Tokyo)* **63**, 375–377 (2010).
27. J.-F. Rontani, A. Mouzdahir, V. Michotey, P. Caumette, P. Bonin, Production of a polyunsaturated isoprenoid wax ester during aerobic metabolism of squalene by *Marinobacter squalenivorans* sp. nov. *Appl. Environ. Microbiol.* **69**, 4167–4176 (2003).
28. Y. Yamada, H. Motoi, S. Kinoshita, N. Takada, H. Okada, Oxidative degradation of squalene by Arthrobacter species. *Appl. Microbiol.* **29**, 400–404 (1975).
29. G. Wang, H. Ran, J. Fan, N. P. Keller, Z. Liu, F. Wu, W.-B. Yin, Fungal-fungal cocultivation leads to widespread secondary metabolite alteration requiring the partial loss-of-function VeA1 protein. *Sci. Adv.* **8**, eabo6094 (2022).
30. K. Dekermendjian, R. Shan, M. Nielsen, M. Stadler, O. Sterner, M. R. Witt, The affinity to the brain dopamine $D_1$ receptor in vitro of triprenyl phenols isolated from the fruit bodies of *Albatrellus ovinus*. *Eur. J. Med. Chem.* **32**, 351–356 (1997).
31. Q. Li, C. Chen, Y. He, M. Wei, L. Cheng, X. Kang, J. Wang, X. Hao, H. Zhu, Y. Zhang, Prenylated quinolinone alkaloids and prenylated isoindolinone alkaloids from the fungus *Aspergillus nidulans*. *Phytochemistry* **169**, 112177 (2020).
32. P. E. A. Teal, D. Jones, G. Jones, B. Torto, V. Nyasembe, C. Borgemeister, H. T. Alborn, F. Kaplan, D. Boucias, V. U. Lietze, Identification of methyl farnesoate from the hemolymph of insects. *J. Nat. Prod.* **77**, 402–405 (2014).
33. M. T. Nielsen, M. L. Klejnstrup, M. Rohlfs, D. C. Anyaogu, J. B. Nielsen, C. H. Gotfredsen, M. R. Andersen, B. G. Hansen, U. H. Mortensen, T. O. Larsen, *Aspergillus nidulans* synthesize insect juvenile hormones upon expression of a heterologous regulatory protein and in response to grazing by *Drosophila melanogaster* larvae. *PLOS ONE* **8**, e73369 (2013).
34. S. Mawa, I. Jantan, K. Husain, Isolation of terpenoids from the stem of Ficus aurantiaca griff and their effects on reactive oxygen species production and chemotactic activity of neutrophils. *Molecules* **21**, 9 (2016).
35. H. D. S. Siqueira, B. S. Neto, D. P. Sousa, B. S. Gomes, F. V. da Silva, F. V. M. Cunha, C. W. S. Wanderley, G. Pinheiro, A. G. F. Cândido, D. V. T. Wong, R. A. Ribeiro, R. C. P. Lima-Júnior, F. A. Oliveira, α-Phellandrene, a cyclic monoterpene, attenuates inflammatory response through neutrophil migration inhibition and mast cell degranulation. *Life Sci.* **160**, 27–33 (2016).

36. A. A. Brakhage, J. Schuemann, S. Bergmann, K. Scherlach, V. Schroeckh, C. Hertweck, Activation of fungal silent gene clusters: A new avenue to drug discovery. *Prog. Drug Res.* **66**, 3–12 (2008).
37. D. Wang, S. Jin, Q. Lu, Y. Chen, Advances and challenges in CRISPR/Cas-based fungal genome engineering for secondary metabolite production: A review. *J. Fungi* **9**, 362 (2023).
38. M. B. Quin, C. M. Flynn, C. Schmidt-Dannert, Traversing the fungal terpenome. *Nat. Prod. Rep.* **31**, 1449–1473 (2014).
39. R. A. González-Hernández, N. A. Valdez-Cruz, M. L. Macías-Rubalcava, M. A. Trujillo-Roldán, Overview of fungal terpene synthases and their regulation. *World J. Microbiol. Biotechnol.* **39**, 194 (2023).
40. R. Jaeger, E. Cuny, Terpenoids with special pharmacological significance: A review. *Nat. Prod. Commun.* **11**, 1373–1390 (2016).
41. H. Tao, L. Lauterbach, G. Bian, R. Chen, A. Hou, T. Mori, S. Cheng, B. Hu, L. Lu, X. Mu, M. Li, N. Adachi, M. Kawasaki, T. Moriya, T. Senda, X. Wang, Z. Deng, I. Abe, J. S. Dickschat, T. Liu, Discovery of non-squalene triterpenes. *Nature* **606**, 414–419 (2022).
42. K. Rose, A. Steinbüchel, Biodegradation of natural rubber and related compounds: Recent insights into a hardly understood catabolic capability of microorganisms. *Appl. Environ. Microbiol.* **71**, 2803–2812 (2005).
43. K. Bromann, M. Toivari, K. Viljanen, A. Vuoristo, L. Ruohonen, T. Nakari-Setälä, Identification and characterization of a novel diterpene gene cluster in *Aspergillus nidulans*. *PLOS ONE* **7**, e35450 (2012).
44. Y. Matsuda, T. Wakimoto, T. Mori, T. Awakawa, I. Abe, Complete biosynthetic pathway of anditomin: Nature's sophisticated synthetic route to a complex fungal meroterpenoid. *J. Am. Chem. Soc.* **136**, 15326–15336 (2014).
45. N. L. Brock, K. Huss, B. Tudzynski, J. S. Dickschat, Genetic dissection of sesquiterpene biosynthesis by *Fusarium fujikuroi*. *Chembiochem* **14**, 311–315 (2013).
46. D. Cox-Georgian, N. Ramadoss, C. Dona, C. Basu, Therapeutic and medicinal uses of terpenes. *Med. Plants* , 333–359 (2019).
47. M. L. Del Prado-Audelo, H. Cortés, I. H. Caballero-Florán, M. González-Torres, L. Escutia-Guadarrama, S. A. Bernal-Chávez, D. M. Giraldo-Gomez, J. J. Magaña, G. Leyva-Gómez, Therapeutic applications of terpenes on inflammatory diseases. *Front. Pharmacol.* **12**, 704197 (2021).
48. Q. Wang, J.-K. Liu, Q. Zhao, Q.-L. He, Mechanistic investigations of hirsutene biosynthesis catalyzed by a chimeric sesquiterpene synthase from *Steccherinum ochraceum*. *Fungal Genet. Biol.* **161**, 103700 (2022).
49. K. Shimizu, N. P. Keller, Genetic involvement of a cAMP-dependent protein kinase in a G protein signaling pathway regulating morphological and chemical transitions in *Aspergillus nidulans*. *Genetics* **157**, 591–600 (2001).
50. V. K. Okura, R. S. C. de Souza, S. F. de Siqueira Tada, P. Arruda, BAC-pool sequencing and assembly of 19 Mb of the complex sugarcane genome. *Front. Plant Sci.* **7**, 342 (2016).
51. S. Warming, N. Costantino, D. L. Court, N. A. Jenkins, N. G. Copeland, Simple and highly efficient BAC recombineering using galK selection. *Nucleic Acids Res.* **33**, e36 (2005).
52. M. T. Robey, R. Ye, J. W. Bok, K. D. Clevenger, M. N. Islam, C. Chen, R. Gupta, M. Swyers, E. Wu, P. Gao, P. M. Thomas, C. C. Wu, N. P. Keller, N. L. Kelleher, Identification of the first diketomorpholine biosynthetic pathway using FAC-MS technology. *ACS Chem. Biol.* **13**, 1142–1147 (2018).
53. K. D. Clevenger, R. Ye, J. W. Bok, P. M. Thomas, M. N. Islam, G. P. Miley, M. T. Robey, C. Chen, K. Yang, M. Swyers, E. Wu, P. Gao, C. C. Wu, N. P. Keller, N. L. Kelleher, Interrogation of benzomalvin biosynthesis using fungal artificial chromosomes with metabolomic scoring (FAC-MS): Discovery of a benzodiazepine synthase activity. *Biochemistry* **57**, 3237–3243 (2018).
54. P. J. Cavnar, K. Mogen, E. Berthier, D. J. Beebe, A. Huttenlocher, the actin regulatory protein HS1 interacts with Arp2/3 and mediates efficient neutrophil chemotaxis. *J. Biol. Chem.* **287**, 25466–25477 (2012).
55. K. P. Drees, J. M. Palmer, R. Sebra, J. M. Lorch, C. Chen, C. C. Wu, J. W. Bok, N. P. Keller, D. S. Blehert, C. A. Cuomo, D. L. Lindner, J. T. Foster, Use of multiple sequencing technologies to produce a high-quality genome of the fungus *Pseudogymnoascus destructans*, the causative agent of bat white-nose syndrome. *Genome Announc.* **4**, e00445-16 (2016).


**Acknowledgments:** We thank the University of Wisconsin Carbone Cancer Center Flow Cytometry Laboratory supported by P30-CA014520 for use of its facilities and services. We also thank the University of Wisconsin National Magnetic Resonance Facility at Madison supported by NIH grant R24GM141526 for use of NMR facilities and the University of Wisconsin–Madison Biophysics Instrumentation Facility supported by the University of Wisconsin–Madison and grants BIR-9512577 (NSF) and S10 RR13790 (NIH) for use of UV and CD facilities. **Funding:** This work was supported by the SBIR award from the National Institute of Allergy and Infectious Diseases at the National Institutes of Health under grant 1R44AI140943 (to C.C.W., J.W.B., and N.L.K.), National Institutes of Health R01 grant AI150669-01A1 (to N.P.K.), National Institutes of Health R01 grant 2R01GM112739-05A1 (to N.P.K.), and National CCIH grant 5R01AT009143-19 (to N.P.K. and N.L.K.). **Author contributions:** Conceptualization: S.C.P., B.N.S., F.Y.L., C.C.W., N.L.K., J.W.B., and N.P.K. Methodology: S.C.P., B.N.S., F.Y.L., R.G., R.Y., C.C.W., J.W.B., and N.P.K. Investigation: S.C.P., B.N.S., F.Y.L., R.G., F.A.B., H.C., R.Y., T.D., C.C.W., and J.W.B. Validation: S.C.P., B.N.S., C.C.W., N.L.K., J.W.B., and N.P.K. Formal analysis: S.C.P., B.N.S., and H.C. Resources: S.C.P., B.N.S., H.C., J.W.B., and N.P.K. Data curation: S.C.P., H.C., C.C.W., and N.L.K. Visualization: S.C.P. and B.N.S. Software: H.C. Funding acquisition: C.C.W., N.L.K., J.W.B., and N.P.K. Project administration: R.Y., C.C.W., J.W.B., and N.P.K. Supervision: C.C.W., N.L.K., J.W.B., and N.P.K. Writing—original draft: S.C.P., B.N.S., and J.W.B. Writing—review and editing: S.C.P., B.N.S., F.Y.L., C.C.W., J.W.B., and N.P.K. **Competing interests:** The authors declare the following competing financial interest(s): C.C.W., R.Y., H.C., and T.D. are employees of Intact Genomics, which sells unbiased Random Shear BAC and FAC libraries and services for genome discovery and DNA research, as well as BAC cloning, DNA end repairing, *E. coli* competent cells, and other enzyme kits for DNA and protein research. The authors declare that they have no other competing interests. **Data and materials availability:** All data needed to evaluate the conclusions in the paper are present in the paper and/or the Supplementary Materials.

Submitted 7 September 2023
Accepted 18 January 2024
Published 21 February 2024
10.1126/sciadv.adk7416